

Active Pixel Sensors in ams H18/H35 HV-CMOS Technology for the ATLAS HL-LHC Upgrade

Branislav Ristic^{a,b}, for the ATLAS CMOS Pixel Collaboration

^aCERN, 1211 Genève 23, Switzerland

^bDPNC, Université de Genève, Quai Ernest-Ansermet 24, 1211 Genève 4, Switzerland

Abstract

Deep sub micron HV-CMOS processes offer the opportunity for sensors built by industry standard techniques while being HV tolerant, making them good candidates for drift-based, fast collecting, thus radiation-hard pixel detectors. For the upgrade of the ATLAS Pixel Detector towards the HL-LHC requirements, active pixel sensors in HV-CMOS technology were investigated. These implement amplifier and discriminator stages directly in insulating deep n-wells, which also act as collecting electrodes. The deep n-wells allow for bias voltages up to 150 V leading to a depletion depth of several 10 μm . Prototype sensors in the ams H18 180 nm and H35 350 nm HV-CMOS processes have been manufactured, to assess a potential drop-in replacement for the current ATLAS Pixel sensors, thus leaving higher level processing such as trigger handling to dedicated read-out chips.

Sensors were thoroughly tested in lab measurements as well as in testbeam experiments. Irradiations with X-rays and protons revealed a tolerance to ionizing doses of 1 Grad. An enlarged depletion zone of up to 100 μm thickness after irradiation due to the acceptor removal effect was deduced from Edge-TCT studies. Finally, the sensors showed high detection efficiencies after neutron irradiation to $10^{15} \text{ n}_{\text{eq}} \text{ cm}^{-2}$ in testbeam experiments.

A full reticle size demonstrator chip, implemented in the H35 process is being submitted to prove the large scale feasibility of the HV-CMOS concept.

Keywords: ATLAS, HV-CMOS, pixel sensors, radiation hard detectors

1. HV-CMOS sensors for the ATLAS Inner Tracker

The sensors of the ATLAS¹ Inner Detector, especially the Pixel Detector are located closest to the interaction point, thus experiencing the highest density of particles and radiation levels. After the Phase II upgrade, the LHC² is expected to deliver an integrated luminosity of up to 3000 fb^{-1} to the ATLAS Detector inflicting a total ionizing dose beyond 1 Grad and NIEL³ fluences beyond $10^{16} \text{ n}_{\text{eq}} \text{ cm}^{-2}$ on the innermost Pixel layer [1]. In order to cope with these elevated requirements the Inner Detector will be replaced by a purely silicon based one. For the inner layers high granularity combined with an extremely radiation hard design is necessary while going to larger radii the cost of producing large areas becomes the limiting factor for detector construction.

The High-Voltage CMOS⁴ technology offers a new approach of producing silicon sensors in a process, standardized and widely used by industry for high voltage switching electronics. Deep n-wells implanted in a p-substrate (see

figure 1) provide the detecting pn-junctions, thus acting as collecting electrodes while shielding the electronics on the surface of the sensor from the applied high voltage. The highly doped substrate is intrinsically radiation hard, but provides only shallow depletion zones. For a good SNR⁵, amplification and further electronics are implemented inside the deep n-well.

Current pixel sensors are usually passive and need a dedicated readout chip for signal processing to which they are bump bonded. This process is usually expensive due to the small pixel pitch of 50 μm , but can be avoided by coupling capacitively via gluing. Although in principle possible for passive sensors, the necessary signal size is difficult to reach without on-sensor amplification, as provided by HV-CMOS sensors.

2. Active pixel sensors in the ams 180nm High-Voltage CMOS technology

The prototypes considered in this paper were built in the Austria MicroSystems (ams) 180nm HV-CMOS process H18 based on designs by I. Peric[2]. Deep n-well structures implanted in a low resistivity ($\sim 10 \Omega\text{cm}$) p-type

Email address: bristic@cern.ch (Branislav Ristic)

¹A Toroidal LHC ApparatuS

²Large Hadron Collider

³Non Ionizing Energy Loss

⁴Complementary Metal-Oxide-Semiconductor

⁵Signal to Noise Ratio

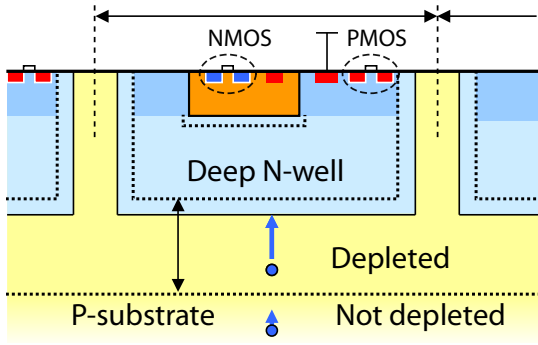


Figure 1: Simplified cross section of an HV-CMOS sensor. The highly sensitive depletion zone grows from the deep n-well implants that shield the electronics sitting on the surface of the chip from the high voltage in the bulk

substrate allow for a bias voltage of up to 95 V which is expected to yield a depletion depth in the order of 10–20 μm . MIP⁶-like particles traversing through that zone would deposit charge with an MPV⁷ of around 600 . . . 1200 electron hole pairs.

The sensors were designed for the latest ATLAS pixel readout chip FE-I4⁸[3] implementing multiple pixel flavors with different optimizations concerning radiation hardness, low noise levels and speed. The default pixel cell combines a charge sensitive amplifier and a source follower with a two stage discriminator. Threshold levels can be set globally with local corrections, applied by setting per pixel DACs⁹. The H18 CCPDv4¹⁰, which will be discussed in this paper, consists mainly of $125 \times 33 \mu\text{m}^2$ pixels of which triples are connected capacitively to one Frontend pad in order to ensure the necessary footprint, as depicted in figure 2. Two Frontend cells, consisting of 6 HV-CMOS sub pixels, form one unit cell. A sub pixel position encoding in the unit cell can be achieved by setting different output levels for the three sub pixels of one Frontend cell and later be decoded by the Frontend’s analog readout. Although in principle possible the encoding was not used for this paper.

Prototypes were irradiated with X-rays and protons at CERN and thermal neutrons at the TRIGA reactor of JSI Ljubljana, Slovenia[4].

3. Irradiation with ionizing particles

Ionizing radiation damages primarily the electronics implanted in the deep n-wells of the HV-CMOS sensors. In order to assess this influence on the ams H18 sensors, prototypes have been irradiated up to 1 Grad TID¹¹ with

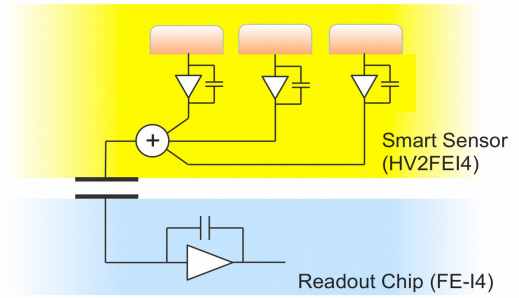


Figure 2: Sketch of an HV-CMOS sensor, capacitively coupled to the Frontend. Three sub pixels are connected additively to one Frontend cell.

X-rays and up to 962 Mrad TID with 24 GeV protons. Irradiations were done in multiple steps, between which the properties of the two types of amplifiers, with linear (LT) or enclosed feedback transistor (ELT), were monitored.

The amplifier output after X-ray irradiation can be found in figure 3. Both amplifiers were functional after 1 Grad, however with a resulting relative amplitude of 88 % for the LT and 45 % for the ELT flavor. Although the irradiated LT showed a higher amplitude it became significantly noisy, while the ELT retained a clean signal. The performance of the ELT amplifier recovered after 25 days of annealing at room temperature with a final amplitude of 62 % after retuning of DAC parameters. Room temperature annealing of the LT amplifier worsened the performance, but was also mitigated by retuning.

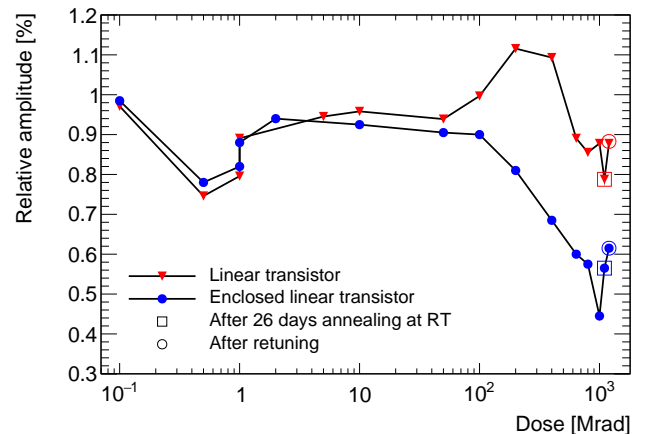


Figure 3: Response of two types of amplifiers, with linear and enclosed feedback transistors to a 1.2V injection pulse after X-ray irradiation up to 1 Grad. The last three points were taken after 1 Grad, but separated for better visibility

When irradiated by protons the performance of both amplifiers is slightly increased between 2 and 50 Mrad and then falls to 75 % as seen in figure 4. As well as for X-rays, the LT becomes noisy after proton irradiation. For this study neither annealing nor retuning was performed. An increase in amplitude after retuning is conceivable.

⁶Minimum Ionizing Particle

⁷Most Probable Value

⁸Frontend-I4

⁹Digital Analog Converter

¹⁰Capacitively Coupled Pixel Detector

¹¹Total Ionizing Dose

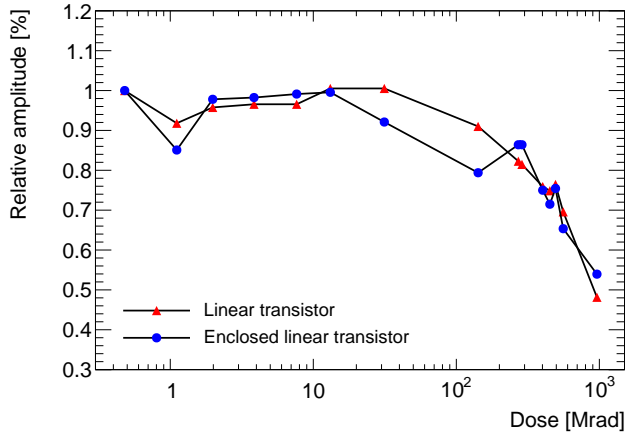


Figure 4: Response of two types of amplifiers, with linear and enclosed feedback transistors to an 1.2 V injection pulse after irradiation with protons up to 962 Mrad

4. Testbeam results

Prototypes of the ams H18 CCPDv4 design were characterized in a testbeam campaign at the CERN SPS¹² H8 180 GeV pion beamline using the FE-I4 beam telescope of University of Geneva. The measurements focused on the STime pixels, that incorporate the newest pixel design. Although in principle possible, no sub pixel encoding was implemented in the DAQ¹³, therefore all sub pixel outputs were set to the same value for a homogeneous signal in the Frontend. This also warranted to merge every pair of FE pixels that corresponds to a unit cell forming virtual pixels of $250 \times 100 \mu\text{m}^2$ size.

Tests were performed on the non irradiated sample 402 and the sample 404 which was irradiated to $1 \cdot 10^{15} \text{ n}_{\text{eq}} \text{ cm}^{-2}$. Due to early breakdown, the maximum voltage was limited to 12 V for 402 and 35 V for 404 instead of 95 V given by design. Discriminators on both sensors were tuned to a threshold close to the noise edge, resulting in an MPV of the threshold of $\approx 300 \dots 500 \text{ e}$. The efficiency vs. virtual pixel position for 402 at its maximum bias voltage is depicted in figure 5. As the measurements focused on the STime pixels, other pixel flavors, implemented on the sensor, were not tuned which results in the low efficiency band at the bottom part of the plot. The upper low efficiency band is the result of a data reconstruction artifact and must not be considered further. For both sensors a bias voltage scan has been performed and the efficiency computed, excluding the discussed artifacts. The non irradiated 402 shows a high efficiency of over 98% already without applied high voltage which increases to 99.7% at 13 V. Sample 404's efficiency raises from $\approx 30\%$ in the unbiased case to 96.2% at 35 V.

This indicates strongly that a big fraction of the charge is collected by diffusion, as after $1 \cdot 10^{15} \text{ n}_{\text{eq}} \text{ cm}^{-2}$ most of

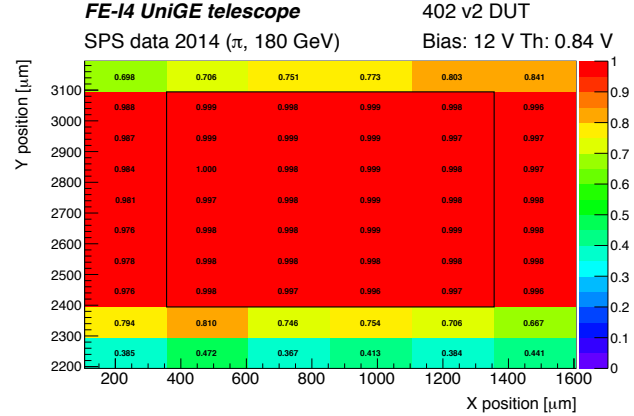


Figure 5: Efficiency map of the non irradiated sample 402. The lower low-efficiency band comes from an untuned pixel flavor while the upper one is a reconstruction artifact. Therefore only the matrix enclosed by the black box was considered for efficiency analysis

the diffusing charge carriers will be trapped, thus not contributing to the signal. By applying a high bias voltage the sensor's performance can be restored. However this could not be tested fully, due to the early breakdown. A significant increase of efficiency can be expected for a properly biased sensor as the data for 404 suggests.

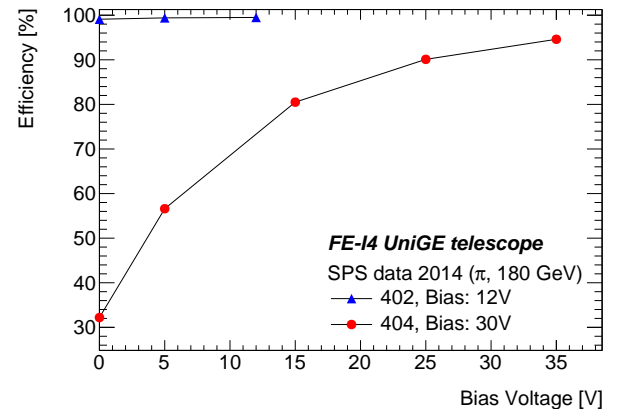


Figure 6: Efficiency with respect to applied bias voltage for 402 and 404 at the highest possible bias voltages

The assumption that diffusion is responsible for a big part of the signal is further supported by timing measurements. Figure 7 shows the distribution of the delay between the detection of the impacting particle by the telescope and the detection by the sensors biased at 5 V. The uncertainty of this measurement is in the order of 20 ns. 402 shows a broadened distribution with a tail towards the higher delay values, while this tail is greatly reduced for 404. Due to the shallow depletion zone little charge is collected by drift. Given a long enough timing window diffusion can drive the signal over threshold, which results in a tail towards higher values. After irradiation the slowly collected charge is trapped, resulting in a significantly improved timing resolution. The remaining inaccuracy is at-

¹²Super Proton Synchrotron

¹³Data Acquisition

tributed to the speed of the amplifier and the response of the discriminator, which has been addressed in the latest prototype versions.

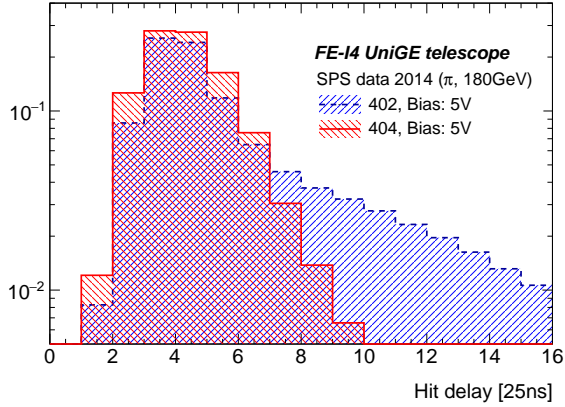


Figure 7: Distribution of the delay time between the telescope trigger and detection in the sensor in units of FE-I4 timing bins [25ns].

5. Edge TCT results on neutron irradiated samples

The Transient Current Technique is a widely used tool for observing time-resolved charge collection in sensors. A typically red or infrared laser induces an electrical signal by ionization of the sensor bulk. Strongly focused lasers provide high spacial resolution and combined with a fast analog readout, movement of charge carriers in the sensor's bulk can be mapped. Usually, the laser is shot through the top or bottom of the sensor. In Edge TCT the laser is shot through a polished side of the sensor, allowing to define the charge deposition depth with a precision in the order of micrometers. A typical experimental setup is sketched in figure 8. [5]

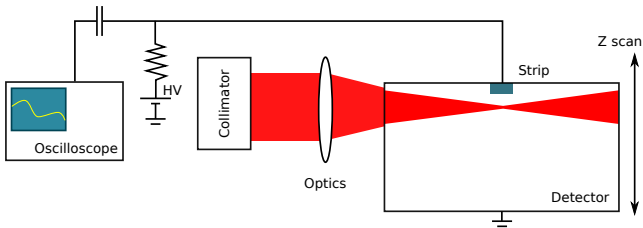


Figure 8: Sketch of a typical Edge TCT setup, consisting of the laser system, fast oscilloscope and biasing electronics

Measurements were conducted on H18 CCPDv3 prototypes, which allow direct access to a $100 \times 100 \mu\text{m}^2$ passive diode at the edge of the chips via a wire bonding pad. It is formed solely by the junction of a deep n-well and the bulk, separated from the fully integrated pixel matrix to avoid influence of the implanted electronics. Samples used for Edge TCT were irradiated with neutrons at the TRIGA reactor of JSI Ljubljana to 1 , 7 and $20 \cdot 10^{15} \text{ n}_{\text{eq}} \text{ cm}^{-2}$.

The analog response to the laser pulses depending on the position and bias voltage was recorded and the charge estimated by integration over the current. Figure 9 shows the collected charge integrated over time for a non irradiated and $7 \cdot 10^{15} \text{ n}_{\text{eq}} \text{ cm}^{-2}$ irradiated sensor. Charge drifting in the high electric field of the depletion zone will be collected quickly forming a steep edge while diffusing charge is collected slowly creating a tail with a low slope. This allows to disentangle the drifting from the diffusing charge by applying a timing cut at $t = 5 \text{ ns}$. Furthermore, as the induced signal at a depth of $30 \mu\text{m}$ shows only a slow charge collection, the depletion depth for the non irradiated sensor is below $30 \mu\text{m}$. In the irradiated case, the signal shows no increase after 5 ns , meaning that most of the diffusing current has been trapped and only charge in the depleted zone and the shallow region around, where diffusing charges can reach the depleted zone before being trapped, is collected. By comparison with the non irradiated data the depletion depth increased after irradiation, which is further investigated by time resolved scans over the depth of the sensor.

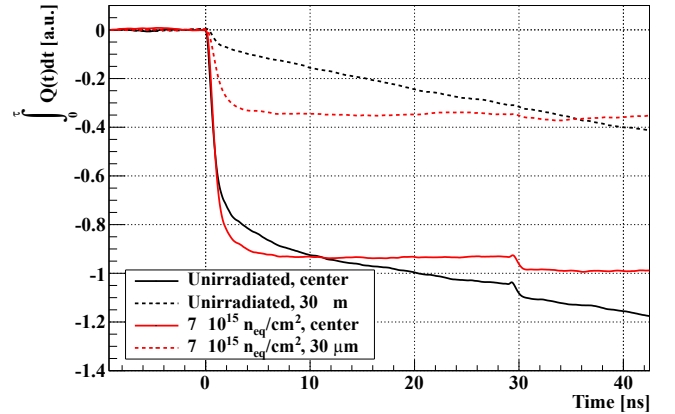


Figure 9: Integrated charge measured in the center of depletion zone and $30 \mu\text{m}$ below for a non irradiated and $7 \cdot 10^{15} \text{ n}_{\text{eq}} \text{ cm}^{-2}$ irradiated sensor. $U_{\text{Bias}} = -80 \text{ V}$, $T = -20 \text{ }^\circ\text{C}$ [6]

The results of these scans in figure 10 reveal the depth profile of the depletion zone. It is shown, that for $1 \cdot 10^{15} \text{ n}_{\text{eq}} \text{ cm}^{-2}$ the width is preserved, whereas the amplitude decreases. After $7 \cdot 10^{15} \text{ n}_{\text{eq}} \text{ cm}^{-2}$ the profile is significantly widened and also the amplitude is increased by $\approx 10 \%$, while for $2 \cdot 10^{16} \text{ n}_{\text{eq}} \text{ cm}^{-2}$ the width is again comparable to the non irradiated case, but here with a significantly reduced amplitude.

The scan over the depth of the sensor simulates a uniform charge deposition in the bulk like it is caused by MIPs. By integrating over the charge profile, the collected charge for a MIP can be assessed. Figure 11 shows this value for different bias voltages. In the case of unbiased sensors, all irradiated samples collect less than 10% of the charge of the unirradiated ones. The $1 \cdot 10^{15} \text{ n}_{\text{eq}} \text{ cm}^{-2}$ and $2 \cdot 10^{16} \text{ n}_{\text{eq}} \text{ cm}^{-2}$ irradiated sensors show a comparable behavior and reach about 90% of the charge collection for 80V. As in the charge profiles, the sensor behaves differ-

ently after $7 \cdot 10^{15} \text{ n}_{\text{eq}} \text{ cm}^{-2}$. The charge collection is on par with the non irradiated one already around 15 V and eventually almost doubles for 80 V.

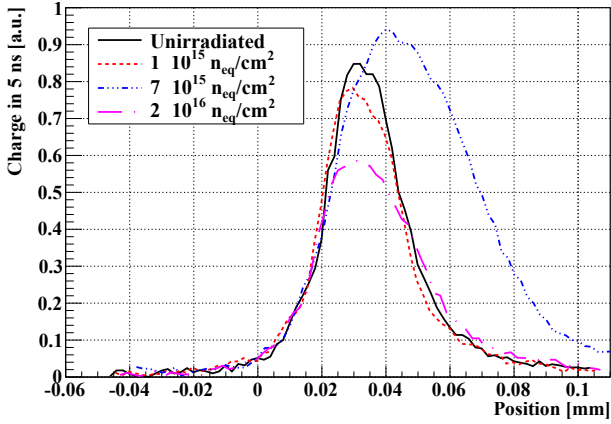


Figure 10: Profile of charge collected in 5 ns for fluences up to $2 \cdot 10^{16} \text{ n}_{\text{eq}} \text{ cm}^{-2}$. $U_{\text{Bias}} = -80 \text{ V}$, $T = -20 \text{ }^\circ\text{C}$ [6]

The influence of radiation on the collected charge can be explained by the acceptor removal effect that occurs in highly doped silicon. Here the effective doping concentration decreases with fluence, leading to an effectively higher resistive substrate, thus a bigger depletion zone at a given bias voltage. The competing trapping effect leads to a decreased collection efficiency after $1 \cdot 10^{15} \text{ n}_{\text{eq}} \text{ cm}^{-2}$. In conjunction with the acceptor introduction effect the active zone is narrowed to the non irradiated width after $2 \cdot 10^{16} \text{ n}_{\text{eq}} \text{ cm}^{-2}$.

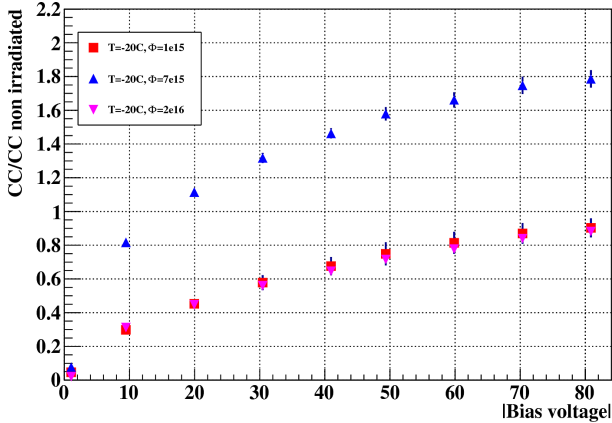


Figure 11: Charge collected in 5 ns integrated over $90 \mu\text{m}$ depth relatively to a non irradiated sensor versus bias voltage. $T = -20 \text{ }^\circ\text{C}$ [6]

Edge-TCT results on irradiated H35 sensors will be soon published in [7] and [8].

6. The ams H35 Demonstrator

The HV-CMOS sensors characterized so far were small prototypes ($\approx 8 \dots 20 \text{ mm}^2$). Based on the promising characterization results and in order to prove the feasibility of

a large scale application, a full reticle size demonstrator chip was designed and submitted through an engineering run. This $18.5 \times 24.4 \text{ mm}^2$ sized sensor incorporates four pixel matrices with $250 \times 50 \mu\text{m}^2$ sized pixels, thus being fully compatible to the FE-I4 footprint (see figure 12). The inner two analog matrices are identical, consisting of 23×300 pixels containing only amplifiers in three flavors, optimized for gain and/or speed. These cells have to be read out by a separate readout chip. The standalone CMOS Matrix consists of 16×300 pixel cells holding amplifiers, which can be additionally read out by CMOS comparators in the periphery of the chip. A digital logic stores the time stamps and generates hit addresses which then can be read out serially at 320 MHz. For the standalone NMOS matrix only NMOS type transistors were implemented. The amplified signals are digitized by in-pixel discriminators and only the digital logic remains at the periphery. All matrices are electrically independent and can be wirebonded and operated separately. The chip has

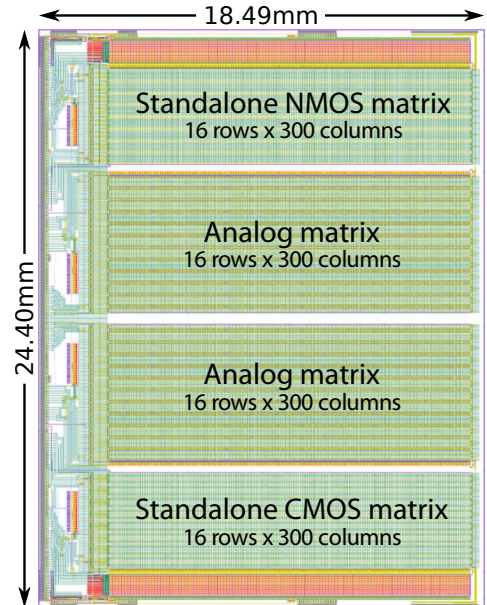


Figure 12: Top view of the demonstrator chip. The four pixel matrices, the separating gap and the standalone readout blocks located at the periphery of the chip are visible.

been submitted on different substrates with resistivities ranging from 20 to $1000 \Omega\text{cm}$. For the higher resistivities, bigger depletion zones, thus increased collected charge is expected. Delivery is envisaged for the end of the year.

7. Summary

Prototypes of the ams HV-CMOS pixel sensors, designed for the Phase-II upgrade of the ATLAS Pixel Detector, were characterized towards performance and radiation tolerance up to 1 Grad TID (X-ray and proton irradiation) and $2 \cdot 10^{16} \text{ n}_{\text{eq}} \text{ cm}^{-2}$ (thermal neutron irradiation). The amplifying electronics remained functional to the highest

applied doses with a reduced gain, which was partially mitigated by room temperature annealing and retuning of the corresponding DAC parameters. Effects of NIEL irradiation were assessed in testbeam and Edge TCT measurements. Although the measured samples could not be biased to the design voltage during the testbeam, the non irradiated as well as the $1 \cdot 10^{15} \text{ n}_{\text{eq}} \text{ cm}^{-2}$ irradiated sensor showed high detection efficiency of over 99 %, respectively 96 %. Edge-TCT revealed a strong, drift based signal after irradiation which drives the charge collection between $1 \cdot 10^{15} \text{ n}_{\text{eq}} \text{ cm}^{-2}$ and $2 \cdot 10^{16} \text{ n}_{\text{eq}} \text{ cm}^{-2}$ even above the non irradiated case. Due to the acceptor removal effect, charge collection for $7 \cdot 10^{15} \text{ n}_{\text{eq}} \text{ cm}^{-2}$ doubles at 80 V bias.

The measurements and improvements over the prototype generations lead to the design and submission of a full reticle size demonstrator to prove the large scale application of these sensors for the ATLAS upgrade.

8. Acknowledgements

The research leading to these results has received funding from the European Commission under the FP7 Research Infrastructures project AIDA grant agreement no. 262025.

References

- [1] ATLAS Collaboration, Letter of intent for the Phase-II upgrade of the ATLAS Experiment, LHCC-I-023 doi: CERN-LHCC-2012-022. URL <https://cds.cern.ch/record/1502664>
- [2] I. Peric, Active pixel sensors in high-voltage CMOS technologies for ATLAS, JINST 7 (08) (2012) C08002. doi:10.1088/1748-0221/7/08/C08002".
- [3] M. Garcia-Sciveres, et al., The FE-I4 pixel readout integrated circuit, NIMA 636 (1, Supplement) (2011) S155 – S159. doi: 10.1016/j.nima.2010.04.101.
- [4] L. Snoj, G. Zerovnik, A. Trkov, Computational analysis of irradiation facilities at the JSI TRIGA reactor, Applied Radiation and Isotopes 70 (3) (2012) 483 – 488. doi:10.1016/j.apradiso.2011.11.042.
- [5] G. Kramberger, et al., Investigation of irradiated silicon detectors by Edge-TCT, IEEE Trans. Nucl. Sci. 57 (2010) 2294. doi: 10.1109/TNS.2010.2051957.
- [6] M. F. Garcia, et al., Radiation hardness studies of neutron irradiated CMOS sensors fabricated in the ams H18 high voltage process, JINST in review. doi:TBA.
- [7] G. Kramberger, I. Mandic, et al., Charge collection studies in irradiated HV-CMOS particle detectors, NIMA in preparation. doi:TBA.
- [8] T. Huffmann, et al., Radiation hardness of two CMOS prototypes for the ATLAS HL-LHC upgrade project, JINST in preparation. doi:TBA.